Available online at www.sciencedirect.com
SCIENCE DIRECT
Thin Solid Films 503 (2006) 85 – 95
thin solid films
www.elsevier.com/locate/tsf

Fractals and superstructures in gadolinia thin film morphology: Influence of process variables on their characteristic parameters

N.K. Sahoo *, S. Thakur [1], R.B. Tokas [1]

Spectroscopy Division, Bhabha Atomic Research Centre, Trombay, Mumbai 400 085, India

Received 15 March 2005; received in revised form 22 September 2005; accepted 29 November 2005
Available online 10 January 2006

Abstract

Characteristic topographic parameters like fractals and superstructures contribute substantially to the thin film morphology, which directly or indirectly influences the physical, optical and mechanical properties. Fractal geometry and scaling concepts can concisely as well as more effectively describe the complex rough surface morphology. In the present study, such microstructural analysis has been carried out for gadolinia thin films, a most promising candidate to develop multilayer optical coatings in the deep ultraviolet spectral region. Extended power spectral density (PSD) spectra for these films acquired through atomic force measurements have been modeled and analyzed using several thin film morphological functions appropriately modified to suit the present requirements. Analysis results of the PSD functions have distinctly indicated the presence of Brownian fractals and uniformly distributed superstructures in the most experimental films deposited through reactive electron beam deposition technique. Process variables such as the rate of deposition and the oxygen partial pressure have affected the microstructural and related morphological evolutions very differently. The rate parameter strongly influenced the intrinsic microroughness, whereas the oxygen pressure influenced the grain sizes of the gadolinia films. One can advantageously use such information in tailoring a desired surface morphology in thin films by choosing appropriate combinations of process variables.

PACS: 42.79 W; 68.35.C; 61.16 C; 81.15E
Keywords: Reactive electron beam evaporation; Surface microroughness; Morphology; Power spectral density; Optical coating; Fractals; Superstructures

1. Introduction

In the case of the thin films obtained through physical vapor deposition (PVD) processes, numerous physical parameters and qualities depend on the structure and the chemical composition [1]. For example refractive index of an optical thin film is intimately associated with the microstructure, void fraction and the packing density with the help of effective medium approximation (EMA) theory [2,3]. Besides, geometric properties like surface morphology or topography have both direct and indirect implications to the structure, quality, performance, physical and optical phenomena in thin films and related multilayer devices. For instance, the intrinsic stress and strain factors in thin films and multilayers predominantly get reflected in the overall morphology [4–6]. The results of various thin film researches indicate that there is a relation between the morphology of the surface of the coatings and the technology used in the process. Due to the random nature of most of deposition processes, the thin films produced are not densely packed and as a consequence have a highly invaginated surface. The contemporary methods used to describe the topography of the surface of the coatings make it possible to define the relation between the process parameters or variables used for the coatings, their structure, usable properties and their morphology evolutions. The description of the complex and disordered surface may be simplified if elements of its symmetry are taken into account. It has also been realized recently that the fractal geometry and scaling concepts can concisely as well as more effectively describe such complex rough surface morphology. The self-affine is one example of the symmetry. The thin film surface morphology at different scales is believed to be self-affine and related to the fractal geometry. Several studies have

* Corresponding author. Fax: +91 22 5505151.
E-mail address: nksahoo@apsara.barc.ernet.in (N.K. Sahoo).
[1] Fax: +91-22-5505151.

0040-6090/$ - see front matter © 2005 Elsevier B.V. All rights reserved.
doi:10.1016/j.tsf.2005.11.107

defended this concept and demonstrated that the complexity of most thin film morphology are indeed fractal in nature, which can be characterized quantitatively by the fractal strengths, indices and their dimensions as well [7–14]. It has also been observed that the non-equilibrium growth fronts of the thin films appear self-affine in spatial as well as in temporal domains. The ability of fractal analyses to extract many different types of information from measured textures compared to common, conventional analyses makes this approach very useful in describing surface characteristics of thin films. Many results demonstrate that fractal structure is a state between order and disorder, which may be unstable in some cases. Films created using two-dimensional ballistic deposition with an isotropic flux (corresponding to a "cosine" angular distribution) have been noticed experimentally to have a characteristic fractal dimension of about 1.5 [15]. For three-dimensional growth cases, Yu and Amar have some very interesting observations while considering the modified ballistic deposition model as a function of the thin film sticking probability. They have distinctly noticed that a surface with fractal dimension D=3 is associated with large sticking probability factor, whereas a flat surface with D=2 has relatively smaller one [16]. In some cases the local grain growth factors can lead to a self assembly of molecules leading to formation of mounds, aggregates or superstructures. Such factors such as the stacking forces between molecules can lead to the appearance of either ordered or ill-defined superstructures. The presence of such superstructures make the thin film morphology more complex to analyze and interpret. These characteristic parameters like fractals and superstructures in the morphology are most preferably estimated with Fourier power spectral density (PSD), which can be acquired through surface characterization techniques such as atomic force microscopy.

In the present work, we have carried out such morphological analyses of gadolinia (Gd_2O_3) thin film systems and noticed a very interesting coexistence of fractals and uniform superstructures in the morphology. The fractal characteristics in thin films appear to be different from the substrate. The substrate morphology in this study depicted marginal fractals in nature. However, effective thin film structures demonstrated more distinct fractal components in the morphology with a fractal dimension approaching 2.5. The nature of these microstructural parameters depicted a strong dependence on the process variables (parameters) used to prepare the thin films. It is also noted that the oxide films obtained through our reactive electron beam deposition process demonstrated the presence of Brownian fractals in the morphology. Such fractals, which carry predominant low frequency components over the higher ones, can favorably lead to reduce optical scatterings in the ultraviolet region. We have also noticed a strong correlation between the refractive index and the fractal strength in these films. Presence of superstructures as seen through the PSD functions indicated their uniform distribution over the morphology. Process variables have shown discerning influences on the sizes, distribution frequencies and roughness contributions due to these superstructures. The following sections give detailed descriptions to the experimental, characterization and the analysis techniques adopted in this study.

2. Importance of gadolinia thin films

Because of the growth in the field of the semiconductor technology, the optical coating requirements in the ultraviolet (UV) and deep ultraviolet (DUV) region have been facing severe challenges to meet the development criteria [17]. For example, deep UV photolithography with an ArF excimer laser source at a wavelength of 193 nm has been identified as a very attractive candidate for this potential process. The most preferable oxide optical coating materials are unsuitable in this spectral region due to their low band gap values. Although fluorides have some favorable transmission properties, because of their poor refractive index ratios an excessive high number of layers are required to achieve the desired reflectivity in this wavelength region. Recently it has been demonstrated that electron beam deposited gadolinia (Gd_2O_3) films under low substrate temperatures can be very conveniently used to 193 nm (ArF laser) spectral region due to its favorable band gap values [1,18]. For a reactively electron beam evaporated gadolinium oxide thin film at low substrate temperature, the process variables like rate and oxygen pressure can have strong influences on the grain structure as well as morphology evolutions. In order to design and develop an efficient low scattered multilayer device, it is essential to explore such parametric dependence of the surface topographies.

3. Microroughness characterization in gadolinia films

Fractals and superstructures contribute substantially to the thin film morphology, which directly or indirectly affects their optical and mechanical properties. Such parameters of an optical surface are most popularly characterized by the power spectral density (PSD) functions. PSD functions describe two aspects of the surface roughness such as the spread of heights from a mean plane, and the lateral distance over which the height variation occurs [19]. Hence, PSD explains a surface much better than the root mean square (RMS) roughness and provides very useful information on fractals and superstructures that may coexist in the microstructures. Such an analysis employing the PSD information over an extended spatial frequency scale has been applied to the present gadolinium oxide thin film surfaces.

As mentioned above, gadolinia films deposited at lower substrate temperature have exhibited high band gaps, which is very useful for developing deep UV optical coatings [1,17]. Hence, in the present study, main thrust has been given to the films deposited under such substrate conditions. Several samples of gadolinium oxide films have been prepared using reactive electron beam evaporation technique by varying the rate and oxygen pressure. The surface height profiles of the films have been measured using atomic force microscopy with different pre-decided scan sizes. The power spectral density

(PSD) functions of all the surface profiles of each film have been computed and combined in to a single PSD profile covering large spatial frequency bandwidth. These experimentally derived PSDs have been fitted with appropriate analytical models. During our investigation, some of the experimental PSD profiles have exhibited more than one local maximum at lower spatial frequency region distinctly suggesting the presence of superstructures in the films. Hence, the existing PSD models have been suitably modified to account for the superstructures present in such thin films. From this modeling, the surface characteristic parameters relating to fractal properties (substrate dominated), roughness information of pure film and superstructures have been obtained for all the gadolinia films. Such information has helped to understand the influence of deposition conditions on microroughness introduced by the fractal components, pure film and the aggregates or superstructures. In addition, one can advantageously use such information in tailoring a surface morphology according to the requirements by choosing appropriate deposition conditions.

3.1. Thin films and extended power spectral density functions

The power spectral density function of thin films can be derived from the measurements of the bi-directional reflectance distribution function or from surface profiles measured by an optical or mechanical profiler or from the atomic force microscopy (AFM) surface profile data [18]. Amongst these techniques, AFM is an excellent tool for characterizing the surfaces and widely being used in studying optical thin film surfaces.

There have been large numbers of publications dealing with PSD calculations from the surface profile data. The computation of PSD function adopted in this paper is given by [20,21],

$$S_2(f_x,f_y) = \frac{1}{L^2}\left[\sum_{m=1}^{N}\sum_{n=1}^{N} Z_{mn} e^{-2\pi i \Delta L\left(f_x m + f_y n\right)} (\Delta L)^2\right]^2 \quad (1)$$

where S_2 denotes the two-dimensional PSD, L^2 is the scanned surface area, N is the Number of data points per line and row, Z_{mn} is the profile height at position (m,n), f_x, f_y are the spatial frequency in the x- and y-directions and $\Delta L = N/L$ is the sampling distance.

This computation is further followed by the transition to polar co-ordinates in frequency space and angular averaging,

$$S_2(f) = \frac{1}{2\pi}\int_0^{2\pi} S_2(f,\varphi)\mathrm{d}\varphi \quad (2)$$

As the PSD function depends on only one parameter, it is plotted in all our figures as a "slice' of the two dimensional representation. It remains a two dimensional function with a unit of fourth power to the length, i.e., "$(\text{length})^4$".

Conventionally, PSD functions obtained from AFM measurements have roughness values in a limited range of spatial frequencies. The range depends on the scan length and sampling distance, and it also can be additionally restricted or constrained by the effect of measurements artifacts. These limitations, however, can be overcome when the topographic measurements performed on different scales are appropriately combined, provided it fulfills the following two conditions.

(i) The spatial frequency ranges where the measurements are defined should partially overlap. The condition is easy to meet by adequate selection of the scan sizes and the sampling distances.
(ii) In the overlapping region, the different PSD functions should be the same order of magnitude.

With these criteria, the combined PSD function at a desired frequency is described by the geometrical average and it is given by,

$$\mathrm{PSD}_{\mathrm{combined}}(f) = \left[\prod_{i=1}^{M} \mathrm{PSD}_i(f)^{1/N}\right] \quad (3)$$

where N is the number of PSD functions overlapping at the concern frequency. In the present work, the measurements have been performed at the same position and with three different scan sizes: 0.45 μm × 0.45 μm, 2 μm × 2 μm and 5 μm × 5 μm. The PSD functions have been computed separately for each scan. The values so obtained have been suitably combined and averaged in order to obtain PSD for the desired extended spatial frequency range. To interpret an experimental PSD function an appropriate analytical model is highly essential providing deep insight to the microscopic parametric dependence like fractals and superstructures. Next section highlights this aspect of model based PSD interpretation.

3.2. PSD models for fractals and superstructures

As described earlier, the PSD contains a more complete description than the RMS roughness and provides useful quantitative information of a thin film surface morphology. However, appropriate analytical models aid to the interpretation and understanding of such morphologies more quantitatively. In the past, several such models have been used to describe specific optical surfaces and thin films. These models consist of a function or combination of functions approximating the experimental PSD functional behavior. The most favorable extended model for the PSD of a thin film coating uses the sum of Henkel transforms of Gaussian and exponential autocorrelation function [22–24]. This model has been extensively used and led to satisfactory results in some specific cases. However, such an approach has a deficiency when wide-range of spatial frequencies is considered. In general, PSD of a thin film coating can be approximated to a sum of PSD of the substrate and the PSD of the pure film [25]. Moreover, in order to describe the surface roughness over large range of spatial frequencies, the PSD analytical model should include the mathematical term describing the overall roughness contribution from the substrate (dominated by fractals), pure film and their superstructures. PSD of the substrates with spatial

frequencies (f) mostly follows a fractal model, which obeys the inverse power law [26], i.e.,

$$\mathrm{PSD}_{\mathrm{fractal}}(f;K,v)=\frac{K}{f^{v+1}} \tag{4}$$

The intrinsic surface parameters describing such fractal-like surfaces are spectral strength (K) and spectral indices (v) rather than RMS roughness (σ) and correlation length (τ). This PSD form is obtained when it is assumed that the surface is self-affine, which is the case with varieties of well-polished (highly finished) substrates. Fractal analysis allows the modeling of such multi-scale nature of self-affine surfaces. The fractal dimension, D, which most is often mentioned by various experimentalists during the PSD analyses, is given using power spectral approach as [27],

$$D=(7-(v+1))/2=(6-v)/2 \text{ with } 0<v<2 \tag{5}$$

The dimension parameter has several significances. It determines the relative amounts of the surface irregularities at different distance scales. For instance under three dimensional growth conditions, the case $D=3$ ($v=0$) is called the extreme fractal; $D=2.5$ ($v=1$) the Brownian fractal; and $D=2$ ($v=2$) the marginal fractal.

Apart from substrate's fractal characteristics, most often, thin film coatings tend to develop fractal structure during the growth stages. The power spectra of most of our experimental PSD profiles of gadolinium oxide films have depicted similar characteristics especially at high spatial frequency regions, which indicate the presence of strong fractal components in the overall thin film topographies. It is, therefore, essential to include an appropriate fractal model to extract roughness contribution of fractal components from the total roughness of such thin films.

The function for describing the PSD of the pure film (i.e., only the film neglecting the substrate) can be conveniently made use of the k-correlation model (also called as ABC model), which is given by [21,28],

$$\mathrm{PSD}_{ABC}=\frac{A}{\left(1+B^2f^2\right)^{(C+1)/2}} \tag{6}$$

with A, B, C being the function parameters and the value of C is greater than 2. This model satisfactorily describes random rough surfaces over large length scales. Eq. (6) gives a PSD function with a "knee," determined by B, which is equal to the correlation length. At small f values, well below the knee or the crossover region, the PSD is determined by A, and at high f values, beyond the knee, the surface is fractal and the PSD function is determined by C. However, the equivalent RMS roughness σ_{ABC} and correlation length τ_{ABC} that depend on these three parameters can be derived as follows:

$$\sigma_{ABC}^2=\frac{2\pi A}{B^2(C-1)},\quad \tau_{ABC}^2=\frac{(C-1)^2B^2}{2\pi^2c} \tag{7}$$

A closer look at these Eqs. (6) and (7) can reveal that the parameter C provides the possibility of having a continuous transition model between the exponential ($C=2$) and the Gaussian ($C\gg 2$) models.

All the above models are monotonically decreasing functions of spatial frequency and cannot account for any additional morphological features. However, it has been observed that most our experimental thin films show the formation of superstructures uniformly distributed along the surface. This induces local maxima in the lower frequencies of the PSD that cannot be explained by any of such previous models. Modeling of such local maxima in PSDs can be carried out using a Gaussian function with its peak-maximum shifted to a non-zero spatial frequency as follows [29]

$$\mathrm{PSD}_{\mathrm{sh}}(f;\sigma_{\mathrm{sh}},\tau_{\mathrm{sh}},f_{\mathrm{sh}})=\pi\sigma_{\mathrm{sh}}^2\tau_{\mathrm{sh}}^2\exp\left[-\pi^2\tau_{\mathrm{sh}}^2(f-f_{\mathrm{sh}})^2\right] \tag{8}$$

This PSD corresponds to an autocovariance function with the form of a Gaussian multiplied by a cosine. The period of the cosine corresponds to the periodicity of the superstructures in the surface. The period is translated into the spatial frequency domain as the shift of the PSD maximum to the frequency f_{sh}. The meaning of the other model parameters can also be related to the various other characteristics of these superstructures. For example here, τ_{sh} corresponds to the size and σ_{sh} to the height of the superstructures.

In order to describe the PSD over a large spatial frequency bandwidth, Ferre-Borrull et al. [21] have used a model that includes Eqs. (4), (6), (8). With this PSD model, they have satisfactorily characterized the surface topographies of ion beam sputtered MgF_2 thin film coatings. The PSD model used by them describes the experimental PSD behavior when there is only one local maximum in the profile. However, the most evaporated films like ours often exhibit superstructures having different values σ_{sh} and τ_{sh} distributed over the film surfaces. For such films, PSD exhibits more than one local maximum, which cannot be described using the above formalism. However, by adopting a combination of shifted Gaussian functions along with fractal and k-correlation functions it is possible to explain the presence of multiple local maxima. In the present investigation, such a multi peak-shifting Gaussian model approach has been employed, which is given by,

$$\mathrm{PSD}_{\mathrm{total}}=\frac{K}{f^{v+1}}+\frac{A}{\left(1+B^2f^2\right)^{(C+1)/2}}+\sum_m\pi\sigma_{\mathrm{sh},m}^2\tau_{\mathrm{sh},m}^2\exp\left[-\pi^2\tau_{\mathrm{sh},m}^2\left(f-f_{\mathrm{sh},m}\right)^2\right] \tag{9}$$

It can be emphasized here that the first term concerned with the fractal function takes into account the substrate as well as substrate induced influences. Where as, the second term representing the ABC model is directly related to the intrinsic roughness of the thin film. The experimental PSD curves of our gadolinia films have been fitted with this modified analytical model. As an example of this analysis method, experimental PSD of the films deposited at two different parametric conditions and their fitting results are presented in Fig. 1(a) and (b). The fractal roughness components of substrate, intrinsic film roughness and superstructures have been derived

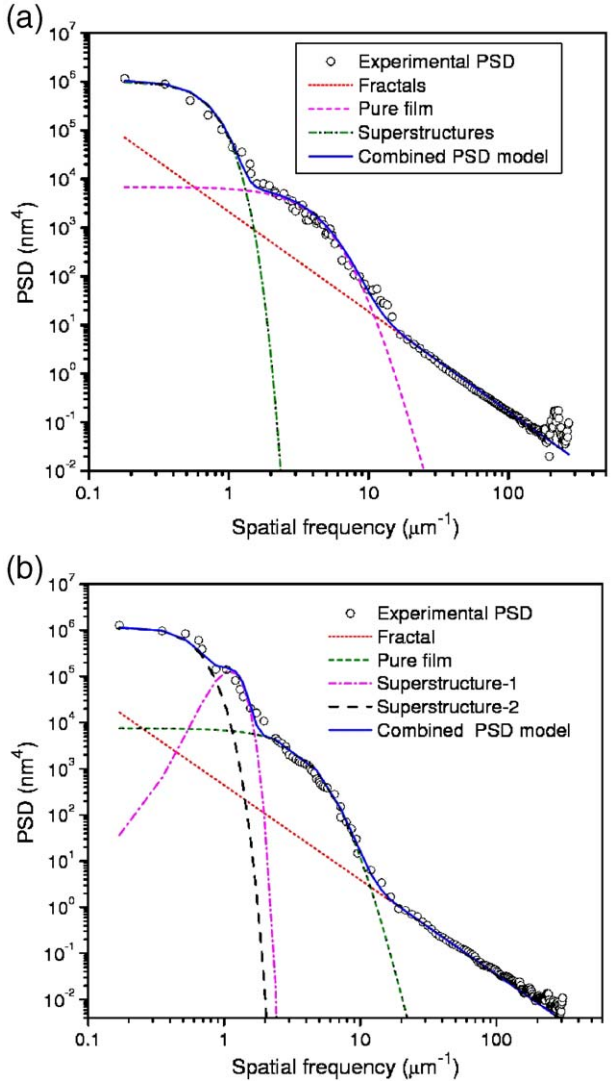

Fig. 1. Fitting of measured PSD of gadolinium oxide films using analytical models that consist of (a) one shifted Gaussian and (b) two shifted Gaussian, along with the fractal and *ABC* functions.

from this modeling. In Fig. 1(a) a local maximum at spatial frequency of 0.183 μm^{-1} is exhibited in the experimental PSD curve. However, in Fig. 1(b), two local maxima have been exhibited at 0.185 μm^{-1} and 1.1 μm^{-1} depicting the presence of multiple superstructures. The goodness of the fit justifies the use of present analytical model for our evaporated films.

4. Experimental details

4.1. Sample preparation

Several thin film samples of Gd_2O_3 films have been deposited on quartz substrate using reactive electron beam evaporation techniques having the optical thickness of $8\lambda/4$ (at $\lambda = 600$ nm). Optical thickness of the films has been monitored using Leybold's OMS-2000 optical monitor. The rates of evaporation have been monitored as well as controlled using Inficon's XTC/2 quartz crystal monitor. During the deposition, the evaporation rate has been varied from 5Å/s to 20 Å/s. However, the oxygen pressure has been varied from 0.5×10^{-4} mbar to 2.0×10^{-4} mbar. Most of the films in the present study were deposited at the substrate temperature of 70 °C. This is because this film material, according to our earlier studies, was observed to give wide band gap (>6.4 eV) at such low and ambient substrate conditions, which is useful in making thin film optical devices for deep UV optical applications. All the films have been subsequently characterized for surface topography using atomic force microscope.

4.2. Atomic force microscopy characterization

The surface topographic measurements have been carried out using NT-MDT's solver-P47H ambient based multimode atomic force microscope. The contact mode of AFM has been chosen for the topographic measurements. A silicon cantilever having typical radius of curvature of 10 nm, force constant of 0.1 N/m and apex angle of 22° has been used for the measurements. Scans have been made over areas of 0.5×0.5 μm, 2×2 μm and 5×5 μm with the resolution of 256×256 pixels for each film. Subsequently, the PSD functions have been calculated according to Eqs. (1) and (2) for all the scan areas. By combining all the PSD functions according to Eq. (3), a PSD over a large spatial frequency bandwidth has been obtained. This procedure has been adopted for all the films deposited under different deposition conditions.

5. Results and discussions

The experimental PSD functions computed for the gadolinia films have been fitted with the analytical model described in Eq. (9). The least square minimization method has been employed to fit all the experimental PSD curves. The fitting parameters obtained from this procedure are presented in the Table 1. In the present investigation, our prime objective is to study the surface topography of gadolinia films deposited at low ambient substrate temperature conditions. For a comparative study, a few films have also been deposited at elevated substrate temperature also. Such a comparison also highlights the importance and of the choice of lower substrate temperature values for the present gadolinia films intended for UV applications. In order to have the distinct topographic evolutions due to the films, the substrate contributions have been independently acquired and analyzed. Fig. 2 depicts power spectral density of uncoated quartz substrate along with its fitting in accordance with the fractal model given by the inverse power law of Eq. (4). It can be seen from this figure that the experimental PSD data fit very well with this fractal model. The fractal dimension of such a substrate is computed to be 2.12, which indicates that it belongs to the category of marginal fractal. The topography of such an uncoated substrate is presented in Fig. 3. The RMS roughness of such a substrate is observed to be 0.38 nm. Such analysis indicates that the fractal component in thin films sometimes may not have very strong correlation with the substrate fractal properties. Rather, the process and the deposition parameters can substantially influence the origin, nature, dimension as well as the strength of such microstructural qualities. The following

Table 1
Fitting fractal and superstructure coefficients of PSD spectra of Gd_2O_3 films deposited at different process conditions

Sample no.	Deposition conditions			RMS roughness (nm)	Various components responsible for thin film roughness evolution											
					Fractal contributions			Intrinsic contributions (K-correlation) or (ABC model)			Superstructure contributions (shifted Gaussian)					
	Rate (Å/s)	O_2 press. ($\times 10^{-4}$ mbar)	Sub. temp. (°C)		K (10^{-3} nm)	ν	Fractal dimension (D)	A (10^2 nm)	B (nm)	C	Superstructure-1			Superstructure-2		
											σ_1 (nm)	τ_1 (nm)	x_1 (μm^{-1})	σ_2 (nm)	τ_2 (nm)	x_2 (μm^{-1})
1	5	0.8	70	4.27	1.9±0.04	1.00	2.50±0.06	14.5	125	4.6	0.68	280	0.35	–	–	–
2	10	0.8	70	2.44	1.3±0.03	1.02	2.49±0.06	92.0	95	7.0	0.65	230	0.25	–	–	–
3	15	0.8	70	4.33	6.0±0.15	1.00	2.50±0.06	160.0	230	5.0	0.32	280	0.36	0.12	450	2.455
4	20	0.8	70	3.93	8.1±0.20	1.05	2.48±0.06	265.0	225	7.0	0.54	300	0.35	–	–	–
5	10	0.5	70	3.03	0.3±0.01	1.05	2.48±0.06	75.5	130	12.0	0.70	850	0.25	0.19	980	1.1
6	10	0.8	70	2.44	1.3±0.03	1.02	2.49±0.06	92.0	95	7.0	0.65	230	0.25	–	–	–
7	10	1.5	70	2.63	1.5±0.03	1.05	2.48±0.06	65.5	130	10.0	0.66	700	0.26	–	–	–
8	10	2.0	70	4.63	0.5±0.01	1.15	2.43±0.05	105.0	230	5.0	0.60	375	0.19	–	–	–
9	10	0.8	250	9.02	6.0±0.15	1.00	2.50±0.06	99.3	330	2.2	0.5	300	0.30	–	–	–
Substrate				0.38	0.3±0.01	1.75	2.12±0.04	–								

Most of the films can be seen to fit very well with a single or with double shifted-Gaussian terms.

sections present some of the experimental results related to these aspects.

5.1. Temperature dependence of fractals and superstructures

The topographies of the films deposited under elevated substrate temperature conditions have shown distinct morphological changes. Such a measurement result has been compared here with the topographies of films deposited at low ambient conditions. Fig. 4(a) and (b) present the typical topographies of films deposited at the substrate temperatures of 70 °C and 250 °C respectively. During the deposition of these films, the oxygen pressure and rate have been kept at 0.8×10^{-4} mbar and 10 Å/s respectively. In this figure, the topography of the film deposited at high substrate temperature depicts the presence of grains of similar sizes dispersed uniformly over the surface. In addition, they are distributed densely over the substrate. A close look to this morphology can reveal the presence several large superstructures or aggregates in the surface. However, topography of the film deposited at low substrate temperature depicts the grains of various sizes distributed over the surface. In most places the grains are clustered leading to formation of mound structures. These superstructures or aggregates depicted relatively more prominence in the morphology and also highlighted their presence in the PSD analyses. This observation can be attributed to the influence of surface mobility of the adatoms in the nucleation stages of the film growth. More quantitative information has been obtained from the PSD function of these surfaces and their characteristic parameters. The PSD functions computed for these films are presented in Fig. 5. It can be seen from this figure that the PSD function of the film deposited at the high substrate temperature shows slower variation over the spatial frequency suggesting the larger lateral structures (grain size) present in this film than the PSD of the film deposited at low substrate temperature. In addition, mid and high spatial frequency regions depicts larger spectral roughness for the film deposited at elevated substrate temperature. The characteristic parameters extracted for these samples (sample nos. 2 and 9) are presented in the Table 1. The intrinsic roughness parameters σ_{abc} and τ_{abc} calculated using Eq. (7) from the characteristic parameters for the film deposited at high substrate temperature are 0.69 nm and 54.85 nm respectively. Where as, the values of σ_{abc} and τ_{abc} for the film deposited at low ambient substrate temperature are 0.33 nm and 45.49 nm respectively. It can be visualized from the PSD analysis that the film deposited at low substrate temperature yields lower intrinsic film roughness and lateral features compared to films deposited at high substrate temperatures.

In order to make complete the understanding about the surface topographies of these films, it is necessary to analyze the remaining fractal components and superstructures (shifted Gaussian parameters) of the film. The PSDs of both the films exhibit inverse power law variation especially at the high spatial frequency region suggesting the presence of strong fractal components in the surface topographies. The spectral indices (ν) for both films are almost same (see Table 1). This is

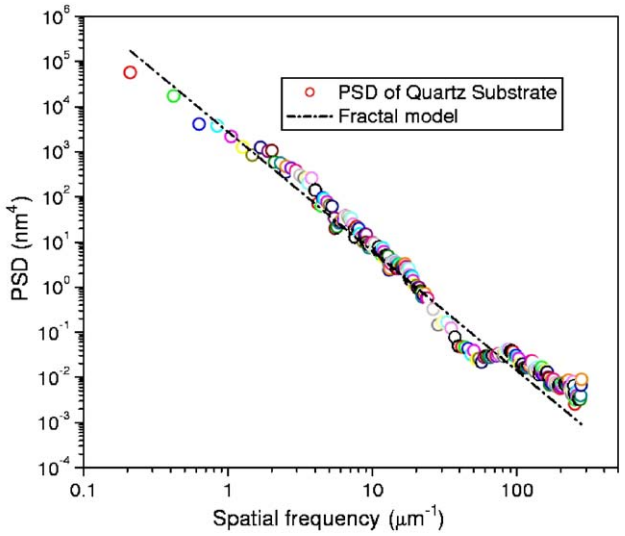

Fig. 2. PSD of uncoated substrate depicting the occurrence of marginal fractals of dimension 1.12.

also evident from the high frequency regions of the PSD curve where the slopes of the PSD curve are same. However, the spectral strength (K) is higher in the case of the film deposited at high substrate temperature. This analysis concludes that the film deposited at higher substrate temperature appears to have stronger fractal components than the low temperature films.

It is well known that the low frequency components of the PSD spectrum represent the aggregates or superstructures. The presence of such superstructures can be seen from the PSD spectra of these films. The low temperature films depicted higher spectral roughness at lower spatial frequency regions suggesting that superstructures have dominantly contributed to the roughness. This observation is a contrast to the film deposited at higher substrate temperatures. However, the intrinsic roughness of the film deposited at low substrate temperatures is small and this justifies our choice of the process variables in preparing these films. Similar analyses have been

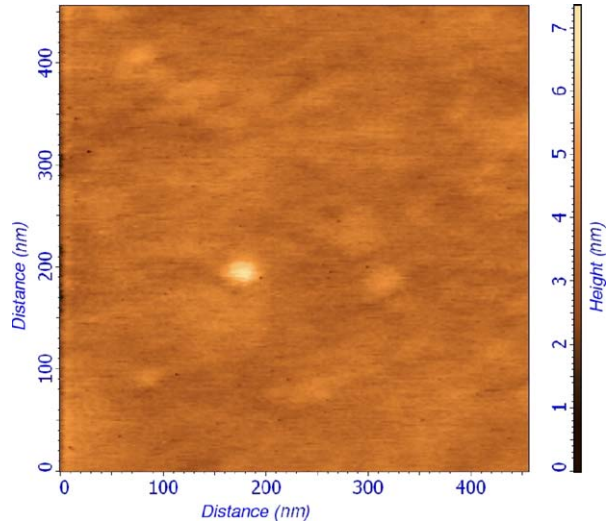

Fig. 3. Topography of uncoated substrate depicting a RMS roughness value of only 0.38 nm.

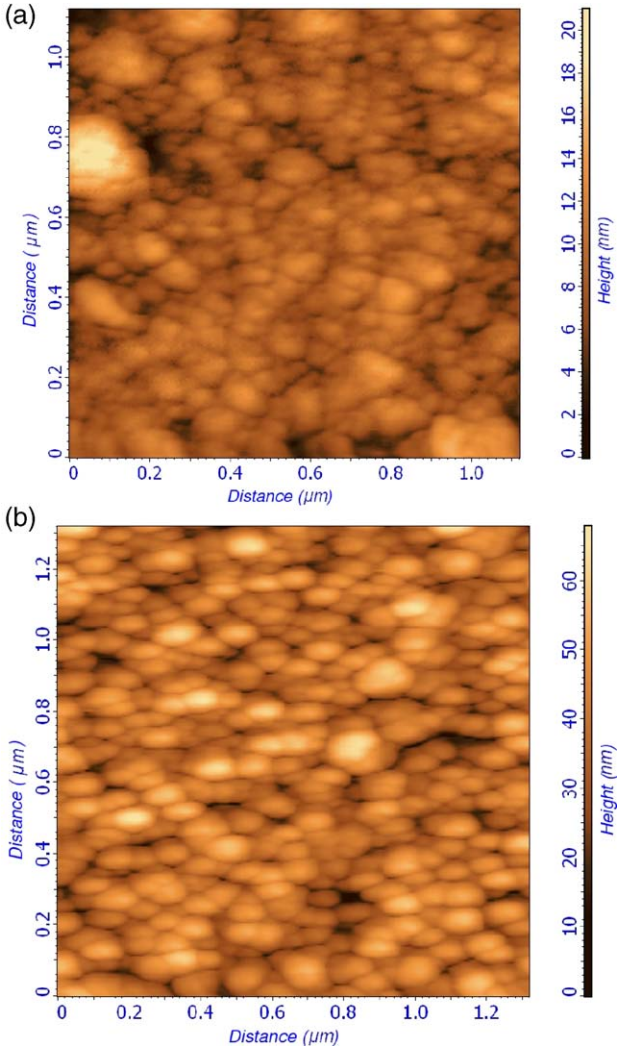

Fig. 4. Surface topography of gadolinium oxide films deposited at the substrate temperature of (a) 70 °C and (b) 250 °C. The scan area is kept at 1 μm × 1 μm.

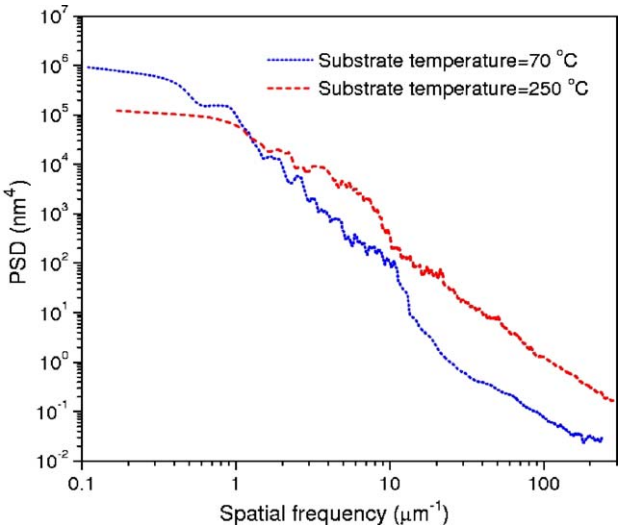

Fig. 5. The experimental PSD profiles of gadolinium oxide films deposited at 70 °C and 250 °C respectively.

carried out for such films deposited at different rates and oxygen pressures. The details of the characterization of these films are presented in the following sections.

5.2. Influence of oxygen pressures

The oxygen pressure during the deposition not only controls the stoichiometry of the films but also influences largely the surface properties. Fig. 6 depicts the PSD profiles of gadolinia films deposited at different oxygen pressures. It can be observed from this figure that the high spatial frequency regions for all films obey the inverse power law variation indicating a presence of strong fractal components in the film topographies. The slopes of the PSDs in this region are almost the same indicating that all the films poses same values of fractal spectral indices (v) or fractal dimensions (D). However, the spectral strength (K) is noticed to vary in this region. In order to confirm this observation and to extract the intrinsic roughness of the films, the PSD profiles have been fitted with the model presented in Eq. (9). The characteristic parameters obtained from the fitting procedure are presented in Table 1. The plot of spectral strength computed for the films deposited at different oxygen pressure is shown in Fig. 7. It can be noted from this figure that the spectral strength is strongly influenced by the oxygen pressure. The lowest value of spectral strength was obtained for the film deposited at the oxygen pressure of 0.8×10^{-4} mbar. However, the spectral indices computed for these films have been noticed to vary from 1.02 to 1.15 implying the dominance of Brownian fractals. One of the noteworthy observations is the relationship between the fractal strength and the refractive indices of the sample films. It can be seen from Fig. 8 that the lower values of the spectral fractal strengths are associated with the higher refractive indices and vice versa. Such an observation highlights a strong correlation between the morphology and the microstructure. This observation is very much similar to the experimental analysis given by Yu and Amar while considering the modified ballistic deposition model for the fractal dimension as a function of the sticking probability [16].

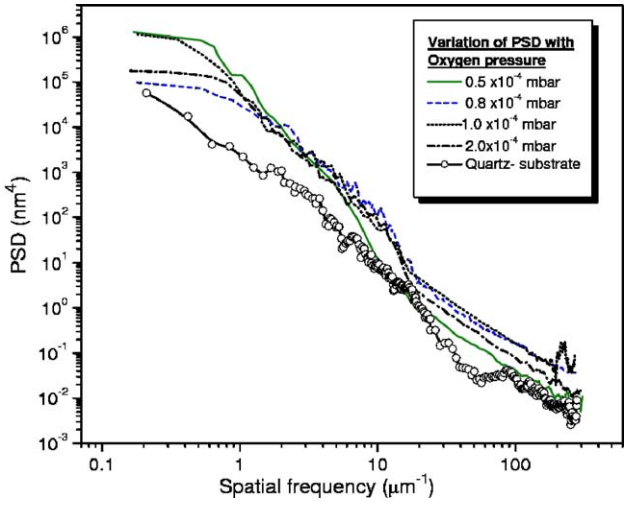

Fig. 6. The experimental PSD profiles of gadolinium oxide films deposited at different oxygen pressures. The rate and substrate temperature during the deposition were fixed at 10 Å/s and 70 °C respectively.

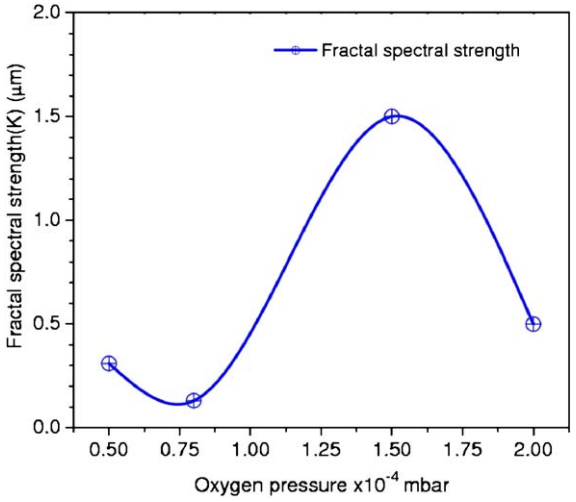

Fig. 7. The variation of fractal spectral strength (K) of the films deposited at different oxygen pressure.

The roughness contribution of the pure film has been extracted using the k-correlation model. The RMS equivalent roughness (σ_{ABC}) and the correlation length (τ_{ABC}) have also been computed from the characteristic parameters obtained from the fitting procedure. The plots of σ_{ABC} and τ_{ABC} with oxygen pressure are presented in Fig. 9. It can be seen from this figure that both surface characteristic parameters have been influenced by the oxygen pressure. Besides, they follow a very similar functional trend. When, high oxygen pressure values have been adopted for the deposition, films have exhibited high values of RMS roughness and correlation length. However, at optimum oxygen pressure (0.8×10^{-4} mbar), films have demonstrated the lowest RMS roughness and correlation length. It can also be observed from this figure that the intrinsic roughness has varied from 0.33 nm to 0.558 nm. However, the correlation length has varied from 45.49 nm to 97.02 nm. It is, therefore, inferred that oxygen pressures alter the lateral features of these films more without causing appreciable changes in the RMS roughness.

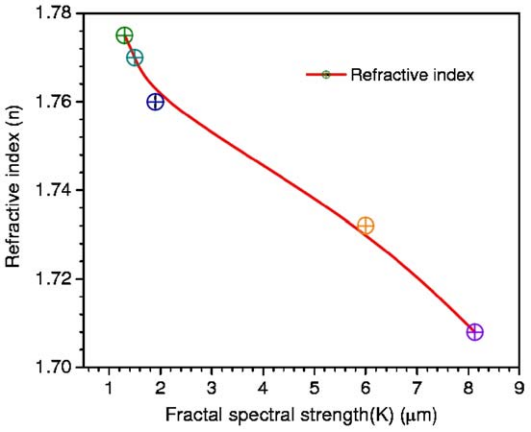

Fig. 8. The variation of refractive indices of the gadolinia films with fractal strength.

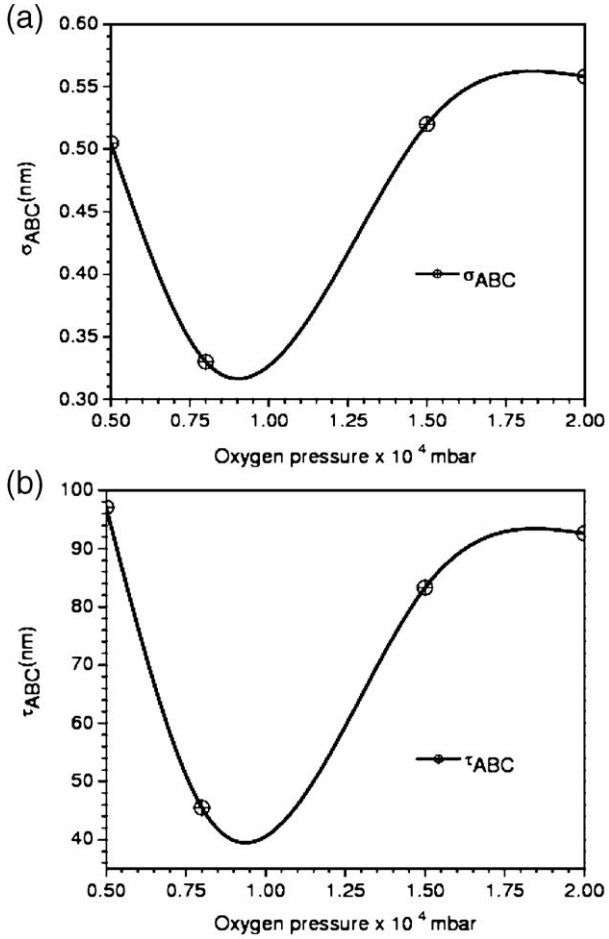

Fig. 9. Plots depicting the variation of (a) roughness (σ_{ABC}) and (b) correlation length (τ_{ABC}) with different oxygen pressures.

5.3. Influence of the rates of deposition

The rate of evaporation has also influenced the surface properties of the gadolinia films to a great extent. Fig. 10

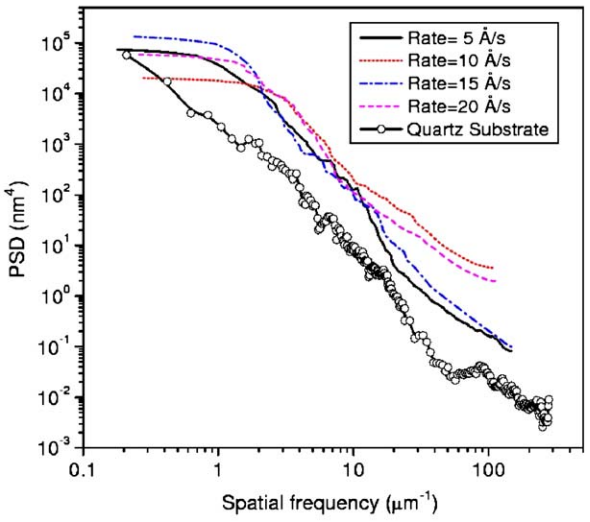

Fig. 10. The experimental PSD profiles of gadolinium oxide films deposited at different rates of evaporation. The oxygen pressure and substrate temperature during the deposition were fixed at 0.8×10^{-4} mbar and 70 °C respectively.

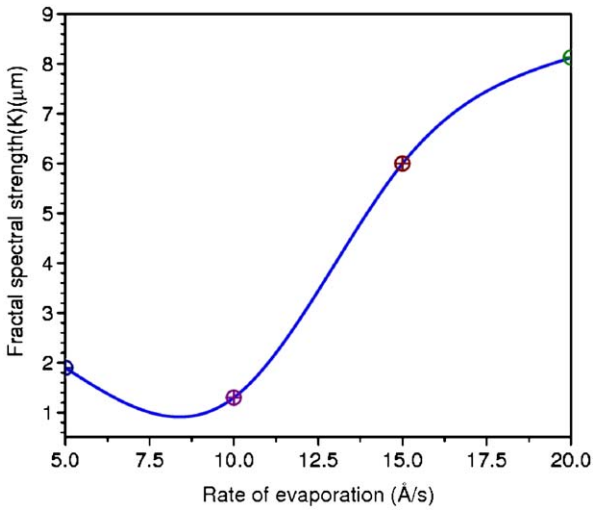

Fig. 11. The variation of fractal spectral strength (K) of the films deposited at different rates of evaporation.

presents the PSD profiles of gadolinia films deposited at different rates of evaporation. Both the high and low spatial frequency regions of the PSD were found to be highly influenced by the rate. However, the medium frequency region is not very much affected by this deposition parameter. It can be observed from this figure that the high spatial frequency region of PSD for all films also obeys the inverse power law variation indicating

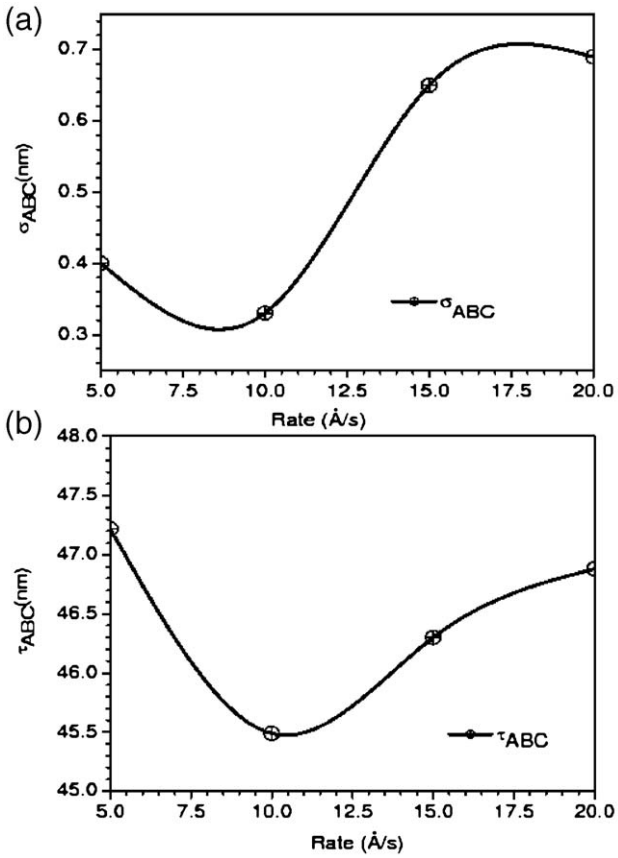

Fig. 12. Plots depicting the variation of (a) roughness (σ_{ABC}) and (b) correlation length (τ_{ABC}) with different rates of evaporation.

the strong presence of fractal components. Besides, the slope of the PSD in this region is almost the same indicating that all the films pose same values for the fractal spectral indices (v) or fractal dimensions (D). However, the spectral strength (K) was observed to vary in this spectral region. As mentioned earlier, the lower spatial frequency part of PSD function predominantly represents the aggregates and superstructures. It can be observed from this frequency region that superstructures contribute to the total film roughness to a large extent. As mentioned earlier, in order to get the complete information about the surfaces, the PSD profiles were fitted with the model presented in Eq. (9). The characteristic parameters obtained from the fitting procedure are presented in Table 1. The plot of spectral strength computed for the films deposited at different rate is shown in Fig. 11. The spectral strength (K) is observed to vary from 1.3 μm to 8 μm with rate of evaporation. The lowest value of spectral strength is obtained for the film deposited at the rate of 10 Å/s. However, the spectral indices computed for these films vary from 1.0 to 1.05. It is important to note that the fractal dimensions (D) for the films deposited under different oxygen pressures and rates have depicted values close to 2.5 indicating the presence of the Brownian fractals. However, the spectral strength has been more influenced by the deposition rate variable than the oxygen pressure. It is therefore concluded that the deposition rate alters the fractal property more prominently than the oxygen pressure.

The roughness contribution of the pure film has also been extracted using the k-correlation model (ABC model). The RMS equivalent roughness (σ_{ABC}) and the correlation length (τ_{ABC}) have also been computed from the characteristic parameters obtained from Eq. (7). The plots of σ_{ABC} and τ_{ABC} with rate of evaporation are presented in Fig. 12. Both the parameters shown in this figure have been influenced by the deposition rate. In addition, both the parameters also follow the similar trends with the rate variation. With our present extreme rates of evaporation, the films have exhibited larger values in RMS roughness and correlation length. However, at optimum rate (10 Å/s), films yielded the lowest RMS roughness and correlation length. It can also be observed from this figure that the intrinsic roughness has

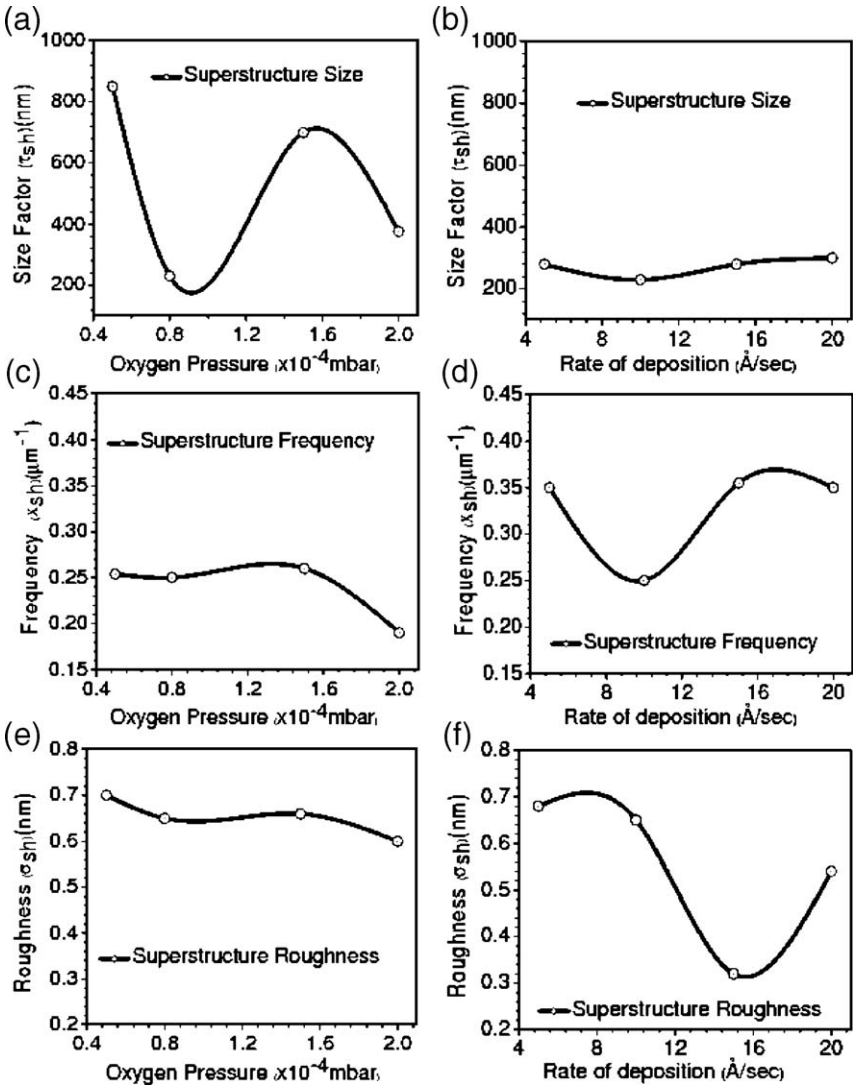

Fig. 13. Plots depicting variation of superstructures sizes with respect to (a) oxygen pressure and (b) rate of evaporation, their periodicity or frequency with different (c) oxygen pressure and (d) rate of evaporation as well as the roughness contributed by these superstructures with different (e) oxygen pressure and (f) rate of deposition.

been varied from 0.33 nm to 0.685 nm. However, the correlation length has been varied only from 45.49 nm to 47.22 nm. It is, therefore, inferred that rate parameter alters the vertical features (RMS roughness) of the film appreciably without causing much change in sizes of the lateral features of the films. This observation is contrary to the influence of oxygen pressure on the film topography.

5.4. Influence of process variables on superstructure parameters

As mentioned earlier, like fractals, superstructures (or grain clusters) can also have dominant contributions in deciding surface quality as well as roughness factors. In the present investigation, both rate and oxygen pressures have influenced the formation of aggregates or superstructures. It is interesting to note that these process variables have shown very similar effects on the superstructure parameters as in the case of fractals. Variation of oxygen pressure has caused the formation of superstructures with sizes (τ_{sh}) ranging from 230 nm to 850 nm (Fig. 13(a)). Whereas the rate variation has caused the formation of such aggregates with sizes (τ_{sh}) ranging only from 230 nm to 300 nm (Fig. 13(b)). Their periodicity or frequency factor has shown a small variation from 0.19 to 0.26 μm^{-1} (Fig. 13(c)) with respect to the oxygen pressure. However, such a frequency parameter has shown relatively more variations with respect to the rate parameter from 0.25 to 0.355 μm^{-1} (Fig. 13(d)). It can be easily visualized from these results that oxygen pressure has caused a large variation in the sizes of superstructures (τ_{sh}) in the present thin film morphologies. In addition, such superstructures have shown to be relatively coarsely distributed over the surface. But such a parameter has not influenced the change in the roughness factors as depicted in Fig. 13(e). On the contrary, the rate variation has depicted appreciable influences on roughness contributions due to the superstructures (Fig. 13(f)). It has also affected relatively more to the distribution frequency of such superstructures leading to a denser morphology. Such results have very close similarities to that observed in the case of fractal analyses. While considering the ultraviolet applications that desire a smaller optical scattering factor, one has to appropriately optimize these process variables for fractal and superstructures leading to a minimum surface roughness value.

6. Conclusion

Reactive electron beam evaporated gadolinium oxide films have exhibited several interesting surface topographies. The effect of rate and oxygen pressure on surface morphologies has been studied using detailed power spectral density analyses. The extended PSD profiles and the interpretation using the analytical models have yielded several interesting information about the fractals, intrinsic film roughness and superstructures of the thin film samples. The oxygen pressure depicted a strong influence on the grain sizes of the pure film than the microroughness. On the other hand, rate variable has portrayed higher influence on the microroughness than the grain sizes of the pure film. The morphology of the films deposited under various rates and oxygen pressures appeared to be mostly of Brownian fractal in nature with dimension close to 2.5. Whereas the topography of the substrate depicted mostly a marginal fractal characteristic with dimension close to 2. The spectral strength (K) of the fractal components of the thin film surfaces have been influenced more by the rate than the oxygen pressure. Both these parameters were found to influence the superstructure formation in the thin film during the growth process. Oxygen pressure has influenced appreciably the size factors of the superstructures than the rate parameter. In addition, fractal spectral strength has been strongly correlated with the refractive index of the film. In the present study, it has been inferred that by systematically varying the process conditions, it is possible to achieve a relatively smooth morphology with an optimum set of deposition parameters. It is evident from our study that the optimum deposition condition (oxygen pressure = 0.8×10^{-4} mbar and rate = 10 Å/s) yields this type of smooth and desirable morphology with the appropriate fractals and superstructures. Such process optimization is very essential to develop low scatter optical coatings for UV and deep UV laser applications.

References

[1] N.K. Sahoo, M. Senthilkumar, S. Thakur, D. Bhattachryya, N.C. Das, Appl. Surf. Sci. 200 (2002) 219.
[2] D. Bruggeman, Ann. Phys. (Leipz.) 24 (1935) 636.
[3] D.E. Aspnes, J.B. Theeten, F. Hottier, Phys. Rev., B 20 (1979) 3292.
[4] N. Sridhar, J.M. Rickman, D.J. Srolovitz, J. Appl. Phys. 82 (1997) 4852.
[5] L.E. Shilkrot, D.J. Srolovitz, J. Tersoff, Appl. Phys. Lett. 77 (2000) 304.
[6] Z. Huang, R.C. Desai, Phys. Rev., B 67 (2003) 075416.
[7] Y. Wang, K.-W. Xu, Thin Solid Films 468 (2004) 310.
[8] J.M. Li, L. Lu, Y. Su, M.O. Lai, Appl. Surf. Sci. 161 (2000) 187.
[9] S.M. Hou, M. Ouyang, H.F. Chen, W.M. Liu, Z.Q. Xue, Q.D. Wu, H.X. Zhang, H.J. Gao, S.J. Pang, Thin Solid Films 315 (1998) 322.
[10] W. Kwa'sny, L.A. Dobrza'nski, M. Pawlyta, W. Gulbi'nski, J. Mater. Process. Technol. 157–158 (2004) 188.
[11] S. Zerkout, S. Achour, A. Mosser, N. Tabet, Thin Solid Films 441 (2003) 135.
[12] J.E. Yehoda, R. Messier, Appl. Surf. Sci. 22–23 (1985) 590.
[13] G. Dumpich, S. Friedrichowski, Thin Solid Films 260 (1995) 239.
[14] F. Wu, J. Zhang, G. Bian, Z. Wu, Commun. Nonlinear Sci. Numer. Simul. 6 (2001) 61.
[15] J. Yu, J.G. Amar, Phys. Rev., E 66 (2002) 021603.
[16] J. Yu, J.G. Amar, Phys. Rev., E 65 (2002) 060601.
[17] A. Duparré, in: R.F. Hummel, K.H. Guenther (Eds.), 1st edition, Hand Book of Optical Properties, vol. 1, CRC Press, Tokyo, 1995, p. 273, Chap. 10.
[18] N.K. Sahoo, S. Thakur, M. Senthilkumar, D. Bhattacharyya, N.C. Das, Thin Solid Films 440 (2003) 155.
[19] J.M. Elson, J.M. Bennett, Appl. Opt. 34 (1995) 201.
[20] C. Rubbe, A. Duparré, Thin Solid Films 288 (1996) 8.
[21] J. Ferre-Borrull, A. Duparré, E. Quesnel, Appl. Opt. 40 (2001) 2190.
[22] J.M. Elson, J.M. Bennett, J. Opt. Soc. Am. 69 (1979) 31.
[23] J.M. Elson, J.P. Rahn, J.M. Bennett, Appl. Opt. 19 (1980) 669.
[24] J.M. Elson, J.P. Rahn, J.M. Bennett, Appl. Opt. 22 (1983) 3207.
[25] S. Jakops, A. Duparre, H. Truckenbrodt, Appl. Opt. 37 (1998) 1180.
[26] E.L. Church, Appl. Opt. 22 (1988) 1518.
[27] A. Mannelquist, N. Almquist, S. Fredriksson, Appl. Phys., A 66 (1998) S891.
[28] G. Palasantzas, Phys. Rev., B 48 (1993) 14472.
[29] G. Rasigni, F. Varnier, M. Rasigni, J. Palmari, A. Llebaria, Phys. Rev., B 27 (1983) 819.